Bahraminasab et al., *BioImpacts,* 2022, 12(3), 247-259
doi: 10.34172/bi.2021.2330
http://bi.tbzmed.ac.ir/

Osteoblastic cell response to Al_2O_3-Ti composites as bone implant materials

Marjan Bahraminasab[1,2*], Samaneh Arab[1,2], Somaye Ghaffari[3]

[1]Nervous System Stem Cells Research Center, Semnan University of Medical Sciences, Semnan, Iran
[2]Department of Tissue Engineering and Applied Cell Sciences, School of Medicine, Semnan University of Medical Sciences, Semnan, Iran
[3]Department of Ceramics, Materials and Energy Research Center, P.O. Box 31787316, Karaj, Alborz, Iran

Article Info

Article Type:
Original Article

Article History:
Received: 30 July 2020
Revised: 14 Nov. 2020
Accepted: 15 Nov. 2020
ePublished: 25 Sep. 2021

Keywords:
Orthopaedic implants
Biocompatibility
In vitro tests
Osteoblast
Al_2O_3-Ti

Abstract

Introduction: Alumina-titanium (Al_2O_3-Ti) composites with enhanced mechanical and corrosion properties have been recently developed for potential applications in orthopaedics and hard tissue replacements. However, before any clinical use, their interactions with biological environment must be examined.

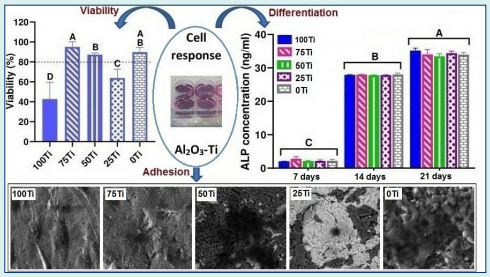

Methods: The aim of this study, therefore, was to assess the biocompatibility of three Al_2O_3-Ti composites having 25, 50, and 75 volume percentages of titanium. These materials were made by spark plasma sintering (SPS), and MC3T3-E1 cells were cultured onto the sample discs to evaluate the cell viability, proliferation, differentiation, mineralization, and adhesion. Furthermore, the apatite formation ability and wettability of the composites were analysed. Pure Ti (100Ti) and monolithic Al_2O_3 (0Ti) were also fabricated by SPS and biological characteristics of the composites were compared with them.

Results: The results showed that cell viability to 75Ti (95.0%), 50Ti (87.3%), and 25Ti (63.9%) was superior when compared with 100Ti (42.7%). Pure Al_2O_3 also caused very high cell viability (89.9%). Furthermore, high cell proliferation was seen at early stage for 50Ti, while the cells exposed to 75Ti proliferated more at late stages. Cell differentiation was approximately equal between different groups, and increased by time. Matrix mineralization was higher on the composite surfaces rather than on 0Ti and 100Ti. Moreover, the cells adhered differently to the surfaces of different biomaterials where more spindle-shaped configuration was found on 100Ti, slightly enlarged cells with dendritic shape and early pseudopodia were observed on 75Ti, and more enlarged cells with long dendritic extensions were found on 0Ti, 25Ti, and 50Ti. The results of EDS analysis showed that both Ca and P deposited on the surfaces of all materials, after 20 days of immersion in SBF.

Conclusion: Our in-vitro findings demonstrated that the 75Ti, 50Ti, and 25Ti composites have high potential to be used as load-bearing orthopedic materials.

Introduction

Nowadays, orthopaedic prosthetic implants are very important because of the increase in the elderly population worldwide which is associated with age-related musculoskeletal pathologies. To enhance the quality of life and healthy ageing, implantable biomaterials with all their forms are used for different purposes, from healing and repair (e.g., scaffolds) to the complete replacement of bones and joints (e.g., total knee and hip replacements).[1,2]

The biological properties of the biomaterials used in bone prostheses should be acceptable to perform successfully after implantation in the body.[3] Ideally, the biomaterial must be non-toxic and provide no adverse effects in-vivo. Various materials including metals, ceramics, polymers, and their composites can all be used to manufacture bone implants.[4-8] Metallic components are employed in most of orthopaedic prostheses among which Ti and its alloys are the most commonly used. Despite many advantages, these

*Corresponding author: Marjan Bahraminasab, Email: m.bahraminasab@yahoo.com

materials are susceptible to corrosion and wear in human body.[9,10] Ions and debris released from the implants into the neighbouring tissues may lead to implant-loosening through stimulating inflammation condition which can activate macrophages and cause bone loss.[11] The application of Ti and its alloys, therefore, has been limited in the load-bearing locations such as femoral condyles of knee prostheses and femoral head of hip implants. The alternative biomaterials based on Ti have been developed to provide improved functioning implants.

Alumina (Al_2O_3) is a ceramic which generates small amounts of wear debris and osteolysis,[12,13] because of its high hardness and low friction coefficient. Furthermore, the Al_2O_3 corrosion resistance and stability in human body can help reducing the ion detachment from Ti implants.[14] Alternatively, Ti can improve the brittleness, and low osseointegration ability of alumina. Therefore, Al_2O_3-Ti composites have been recently made by spark plasma sintering (SPS), and their superior mechanical properties[15-19] and corrosion characteristics[20,21] have been reported. This is due to the advantages of SPS process including high heating rates, achieving fully dense materials in a very short time, and combination of temperature and pressure reducing the phases reactivity in composite materials. In one study, Gutierrez-Gonzalez et al[16] fabricated a composite with 25 vol.% titanium by SPS machine and evaluated its mechanical properties and microstructure. The authors obtained improved flaw tolerance and toughness rather than pure Al_2O_3. Furthermore, in another study[18] a series of Al_2O_3-Ti composites with different metal to ceramic weight ratio was developed using TiH_2 and Al_2O_3 as starting materials. The developed composites were assessed for their phase composition, microstructure, and mechanical behaviour. They found that Ti and Al_2O_3 phases were evenly distributed in the composites, and the increase of modulus of elasticity and hardness, and decrease of fracture toughness with the increase in Al_2O_3 content in the composites. Moreover, similar series of Al_2O_3-Ti composites made by SPS process were analysed for their phase constituents and dynamic response of the composites under loading.[17] Fujii et al[19] also investigated the influence of different raw powders including pure Ti and TiH_2 on the mechanical behaviour of Al_2O_3-Ti composites. Further, Bahraminasab et al[15] fabricated functionally graded and composite Al_2O_3-Ti samples and evaluated their microstructural, physical, and mechanical properties. Their results showed an increase in the strength by the increase of Al_2O_3 percentage. The flexural strengths of 25vol.%Ti, 50vol.%Ti, and 75vol.%Ti were 172.97, 164.28, and 149.98 MPa, respectively. Two studies also assessed the corrosion characteristics of Al_2O_3-Ti composites having 75vol.%Ti and 50vol.%Ti and compared their properties with pure Ti.[20,21] The composites showed high corrosion resistances, particularly 75vol.% Ti. Regarding the biological properties, the only study is that of Guzman et al[22] in which a composite with 25vol.%Ti was investigated for cytotoxicity, and for its effect on cell proliferation, differentiation, and adhesion using pre-osteoblast MC3T3-E1 cell line. Their findings rejected any cytotoxicity of the new composite, and indicated improved proliferation and early-differentiation of the cells.

To the best of the authors' knowledge, the effect of chemical composition of these composites on the biological properties has not been studied yet. In the current study, therefore, different Al_2O_3-Ti composites along with pure Ti and Al_2O_3 were investigated for their apatite formation ability, chemical stability, and osteoblastic cell responses. The composites and pure samples were first fabricated by SPS process and some of them were subsequently subjected to simulated body fluid (SBF) to evaluate their ability to adsorb Ca and P, and some samples were immersed into phosphate-buffered saline (PBS) to assess their chemical stability. The others were subjected to MC3T3-E1 cells to evaluate cell viability, proliferation, differentiation, mineralization, and adhesion at different time points.

Materials and Methods

Sample preparation

Al_2O_3-Ti composites, pure Ti and Al_2O_3 were fabricated using SPS machine (SPS-20T-10, Easy Fashion Metal Products Trade CO. Ltd. China). Almost full dense materials were obtained (Table 1). This was in agreement with our previously published paper,[15] based on which the manufacturing approach was carried out. Briefly, the raw powder of α-Al_2O_3 (particle size: 0.1-3 μm) and Ti powder (particle size: <45 μm) with different volume fractions including 0:100, 25:75, 50:50, 75:25, and 100:0 were used to make the samples. Each mixture of the powders was ball milled (PM400, Retsch, Germany) under the same conditions of 100 rpm rotating speed for 1 hour using zirconia jar and balls. The ball to powder ratio was 5:1. The powders were added into a graphite die having a diameter of 30 mm. The step-wise pressure was applied; 10 MPa for 3 minutes, 20 MPa for the next 10 minutes, and 40 MPa until the end of the SPS process. The sintering temperature and heating rate were 1350°C and 50-100 °C/min, respectively. The soaking time at 1350°C was 3 minutes for the composite and pure Ti specimens and it was 30 minutes for the monolithic Al_2O_3 samples. The provided discs were 3 mm in height.

In vitro bioactivity

To evaluate the ability of the composites, Ti and Al_2O_3 in apatite forming on their surfaces SBF was prepared based on Kokubo and Takadama[23] by sequentially dissolving NaCl, $NaHCO_3$, KCl, $K_2HPO_4.3H_2O$, $MgCl_2.6H_2O$, $CaCl_2$, Na_2SO_4 in distilled water, and buffering the solution to pH=7.4 at 36.5°C by Tris and 1M HCl. All materials were purchased from Merck, Germany. The concentrations of ions in the solution are similar to those of human blood plasma (Na^+:142.0, K^+:5.0, Mg^{2+}:1.5, Ca^{2+}:2.5, Cl^-:147.8, HCO_3^-:4.2, HPO_4^{2-}:1.0, and SO_4^{2-}:0.5 (mM)). To do this

Table 1. Compositions, density, and Ca/P ratios of the samples

Sample codes	Compositions	Measured density (g/mm³)	Theoretical density (g/mm³)	Surface finish	Ca/P (W) at day 20
100Ti	100vol.%Ti	4.47±0.008	4.5	5 microns	0.52±0.21
				grit 1200	0.68±0.49
75Ti	75vol.%Ti-25vol.%Al_2O_3	4.46±0.020	4.37	5 microns	0.46±0.29
				grit 1200	0.28±0.09
50Ti	50vol.%Ti-50vol.%Al_2O_3	4.27±0.008	4.24	5 microns	0.78±0.26
				grit 1200	0.29±0.12
25Ti	25vol.%Ti-75vol.%Al_2O_3	4.06±0.026	4.11	5 microns	1.08±0.59
				grit 1200	0.64±0.22
0Ti	100vol.% Al_2O_3	3.96±0.004	3.98	5 microns	0.39±0.06
				grit 1200	0.78±0.58

test, 2 series of samples (grit 1200 and 5 μm) were used which were cleaned ultrasonically in ethanol (70%) for 10 minutes. Subsequently, after rinsing, they were ultrasonicated in distilled water for another 10 minutes. The samples, then, were dried in a thermostatic oven (Behdad Company, Iran) for 24 hours. In the end, they were immersed in individual containers of SBF solution at 37 ± 0.5°C and kept for 10, 20, and 30 days. The volume of SBF required for the samples were calculated by dividing the apparent surface area of specimen by 10 ($V_{SBF} = \frac{S_{sample}}{10}$). The SBF was refreshed every two days. At the end of the exposure time, the specimens were cleaned three times with distilled water and then dried. Scanning electron microscope or (Philips XL30, the Netherlands) SEM images were taken from the surfaces of the samples before exposure to SBF, and after 10 and 30 days of immersion. Furthermore, the surfaces of materials after 20 days of immersion were analysed by energy-dispersive X-ray spectroscopy or EDS (TESCAN MIRA3 LMU) at several regions on the surfaces of the samples. Atomic Force Microscope (Bio-AFM, Ara-Research Company, Iran) was also employed for imaging the surface topography of the samples before and after 20 days of immersion in SBF. The surfaces were scanned using non-contact mode at the ambient condition. The scanning area was 10 μm × 10 μm. AFM images were analysed by Imager version 1.00 software supplied by Ara-Research Company. The surface roughness values of the samples were also determined by the same software after scanning three regions on the surfaces of each sample. The arithmetical mean deviation of the assessed profile (Ra) and root mean squared roughness (Rq) values were obtained in 10 lines of each image (totally 30 lines for each material). Finally, the mean values and standard deviations (STDVs) were reported.

Chemical stability in phosphate-buffered saline

The specimens were first weighed and ultrasonically cleaned by ethanol and distilled water (10 minutes each), respectively. They were then immersed in PBS individually in separate containers which were kept at 37 ± 0.5°C in a thermostatic oven (Behdad Company, Iran) for 4 weeks. The samples were weighed twice a week. To do this, the samples were first removed from the PBS solution, washed with distilled water, dried in the oven for about 1 hour, and finally weighed.

Wettability test

Liquid–solid contact angle (CA) is a surface characteristic which can affect the biological response.[24] Static water CAs with the surfaces of the samples were measured by the sessile drop method at room temperature. This was done using CA goniometer; the distilled water droplet was deposited automatically by a syringe pointed vertically down onto the specimen surface and a video camera which was situated on the microscope recorded the water drop images immediately after deposition on the surface using DFK 23 USB 3.0 Color Industrial Camera with the help of a 2X lens. For doing this test, the samples were wet grinded (water used as lubricant), and polished up to 5 μm. The samples were then ultrasonically cleaned in ethanol for 20 minutes. Three-four measurements were performed on each specimen at different points. The CA on the right and left sides of the drop, and the drop width and height were measured at each point.

In vitro biocompatibility tests

Samples sterilization

After polishing of the fabricated materials up to 5 μm on all sides, and ultrasonically cleaning with ethanol and distilled water, they were covered by aluminium foil, and sterilized by heating within a hot air oven (Behdad Company, Iran) at 100°C for 1 hour, and immediately transferred to a laminar flow bench to carry out the in-vitro tests.

Cell culture

Pre-osteoblast MC3T3-E1 cell line (Mouse C57BL/6 calvaria, ECACC, Sigma-Aldrich, Sweden) culture was performed in complete Dulbecco's Modified Eagle's medium or DMEM [25] (Gibco Life Technologies; USA). Complete medium of DMEM was prepared by adding 10 vol.% FBS (Gibco Life Technologies; USA), penicillin (100 IU), and streptomycin (100 μg/mL), and 2 mM l-glutamine (Gibco Life Technologies; USA). The cells were cultured in an incubator with a balanced atmosphere of 5% CO_2

and 95% humidity at 37°C. Routine passaging was carried out on flasks by discarding the culture medium, rinsing with PBS, trypsinization, centrifugation, and insertion to new flask/flasks with fresh complete medium.

Cell viability test

Viability of the cells was assessed by a lactate dehydrogenase (LDH) cytotoxicity detection kit (Roche Applied Science, Germany). MC3T3-E1 cells (10^5 cells/well) were seeded in 6-well plates containing the sample discs in complete growth medium (DMEM/F12+10% FBS). After 3 days of incubation with materials, the plates were centrifuged, and the supernatants were transferred to a 96-well ELISA plate. In this test, dilutions of [1:5] and [1:10] were also prepared. The LDH detection mixture was, then, added into the wells (0.1 mL to each well), and the plates were incubated for 30 minutes at room temperature. The absorbance was measured at 490 nm by a microplate ELISA reader (Synergy H1 Hybrid Multi-Mode Microplate Reader, BioTek, USA). The percentage of cell viability was determined by equations 1 and 2.

$$Cytotoxicity(\%) = \frac{experiment\ value - low\ control}{high\ control - low\ control} \times 100 \quad (1)$$

$$Viability(\%) = 100 - Cytotoxicity \quad (2)$$

In this test, low control was prepared by mixing the supernatants of cells cultured without materials with LDH detection mixture, and high control was provided through lysing the cells with triton X-100 provided by the kit.

Cell proliferation

Cell proliferation after 3, 7, and 10 days from plating was assessed by MTT [3-(4,5-dimethylthiazol-2-yl)-2,5-diphenyltetrazolium bromide] cell proliferation kit (Cell Growth Determination Kit, Sigma Life Science) according to the manufacturer's instruction. MC3T3-E1 cells (10^5 cells/well) were seeded in 6-well plates containing the discs of samples in complete growth medium (DMEM +10% FBS). After the incubation (for 3, 7, and 10 days), 100 µL MTT solution was added into each well and incubated at 37°C for 4 hours. At the end of the incubation, 1000 µL of isopropanol containing hydrochloric acid (0.04 N) was added to each well, and the insoluble formazan formed was dissolved by pipetting up and down. Then, 100 µL of solution was transferred to each well of a 96-well ELISA plate (two samples from each material with three replicas in 96-well ELISA plate (6 reads for each material)). The absorbance was measured at 570 nm by a microplate ELSA reader (Synergy H1 Hybrid Multi-Mode Microplate Reader, BioTek, USA). Optical micrographs were also taken after 10 days of exposure.

Cell differentiation and mineralization

MC3T3-E1 cells were seeded on the sample discs at a density of 10^4 cells/well in 6-well plates. Osteogenic factors including ascorbic acid, 50 µg/mL, and β-glycerophosphate, 10mM (Sigma-Aldrich, USA) were added after 72 hours. The ALP activity was evaluated after 7, 14, and 21 days using an Alkaline Phosphatase Colorimetric Assay Kit (SensoLyte pNPP Alkaline Phosphatase Assay Kit, Ana Spec Inc., USA). Osteoblasts were lysed with 1000 µL of Triton X-100 and the cellular extracts were incubated with the colorimetric ALP substrate, pNPP, in 96-well plate for 20 minutes at room temperature. The ALP activity was analysed by measuring the absorbance at 405 nm. The OD values were extrapolated to a calibration curve of ALP standard from calf intestine provided by the kit (the serial dilutions were from 100 to 0 ng/mL). The mineralization (the calcium matrix) was assessed after incubation for 7 and 14 days. The cells on the samples were fixed by 4% paraformaldehyde at 4°C for 20 minutes. The fixed samples were then washed three times with PBS, and the Alizarin Red kit (Kia Zist Company, Iran) was added on the samples and the plate was kept in dark for 40 minutes. The samples were then washed with PBS three times again, and observed under a loop microscope. The percentage of red-stained area on each sample was calculated using Image J software.

Cell adhesion

The ability of the cells to adhere on the surfaces of materials was analyzed using SEM (TEGA//TESCAN, Czech Republic). To this end, 10^3 cells were seeded on the center point of each sample surface and cultured for 72 hours. After the incubation time, the adhered cells were dehydrated with a series of gradient alcohol (30%, 50%, 70%, and 96%) and dried. SEM Images were acquired at different magnifications in the secondary electron (SE) and backscattered electron (BS) modes at an accelerating voltage of 20 kV.

Statistical analysis

Statistical analyses were performed through analysis of variance (ANOVA) using Minitab V17 software. The confidence level in all tests was set to be 95% (α=0.05). The normal probability plot of residuals was checked in all analyses. Furthermore, the post hoc pairwise comparisons were conducted using Tukey test or Games-Howell test depending on the variance homogeneity. The bar charts were provided using GraphPad Prism (version 8).

Results

Apatite forming ability of the materials and chemical stability

The ability of 75Ti, 50Ti, and 25Ti composites to adsorb Ca and P on their surfaces was tested and compared with that of 0Ti and 100Ti samples. The samples were immersed in SBF solution for 10, 20, and 30 days at 37°C. Subsequently, their surfaces were observed by SEM and analyzed by EDS for both grit 1200, and 5 microns polished samples. Fig. 1 represents the SEM images obtained before immersion in SBF and after 10 and 30 days of immersion for grit 1200. The images showed that deposits were formed on the surfaces of all samples. Meanwhile, the amount of mineral deposits increased by time. Small white or light grey spots

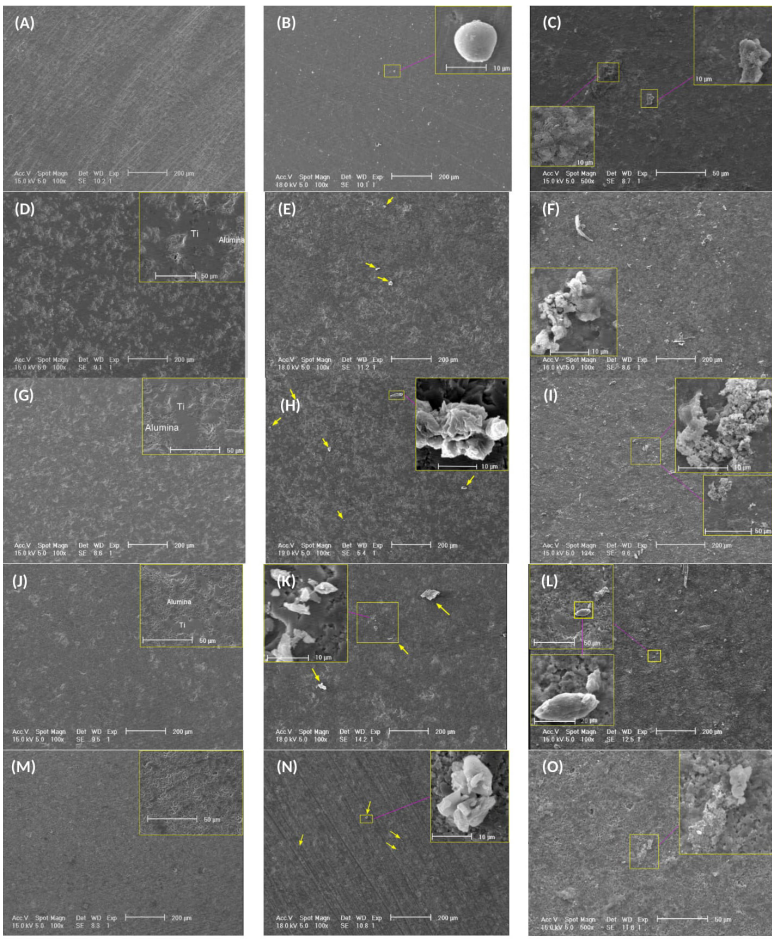

Fig. 1. SEM images of the surfaces of samples; (A-C) 100Ti, (D-F) 75Ti, (G-I) 50Ti, (J-L) 25Ti, (M-O) 0Ti, (A, D, G, J, and M) before immersion, (B, E, H, K, and N) day 10 of immersion, and (C, F, I, L, and O) day 30 of immersion.

in the middle images of Fig. 1 (pointed by arrows) are indicative of the deposits on the surfaces of samples after 10 days of immersion. It seems 100Ti had more deposits on its surface compared to other materials after 10 days of exposure to SBF. After 30 days, however, the deposits increased and grew so that the surfaces of all samples became non-uniform and rough. The EDS analysis 20 days after immersion in SBF indicated that same elements such as Ca, P, K, Mg, Na, and Cl were deposited on all sample surfaces. Fig. 2 shows one of the EDS analyses for 75Ti, 50Ti, and 25Ti. Ca/P ratio is important in the formation of apatite and new bone for which the molar ratio should be 0.58-2.34 (theoretically 1.67) or the mass (weight) ratio should be 1.3-2.2 (theoretically 2.15).[26] The mean values obtained here (both grit 1200 and 5 microns) were lower than the identified range for apatite formation (Table 1), however, some regions on the samples were found with Ca/P ratio within or near the specified range.

The surface roughness and topography of the samples were obtained by AFM after 20 days of immersion. Despite having the same polishing protocol (up to 5 microns) for all specimens, the unlike nature of materials (i.e., pure metal, pure ceramic, and composites) caused differences in topography and roughness. Fig. 3 shows the AFM images taken from the surfaces of the studied materials before and after 20 days of immersion in SBF. It can be seen that the surfaces were rougher after 20 days of exposure to SBF. Fig. 4 compares the mean values of Ra and Rq (as measures of surface roughness) of different materials before and after 20 days of immersion in SBF. As it can be seen in Fig. 4, the surface roughness of all samples increased after immersion where the highest ΔRa and ΔRq belonged to 50Ti, followed by 25Ti. The least ΔRa and ΔRq were obtained for 75Ti.

The chemical stability of the fabricated materials was studied by immersion in PBS for 4 weeks and by regular weighing of the samples. The measured values showed no decrease in the weights of the materials during this time meaning that they were very stable in PBS and did not release any unwanted products.

Wettability of the materials

One-way ANOVA was used to identify the effect of materials compositions on their wettability. The results of Welch's Test on CAs indicated that material was a significant factor ($P = 0.000$). Fig. 5a shows differences between the means of CAs in different materials. As it can be seen in this figure, the lowest CA was associated

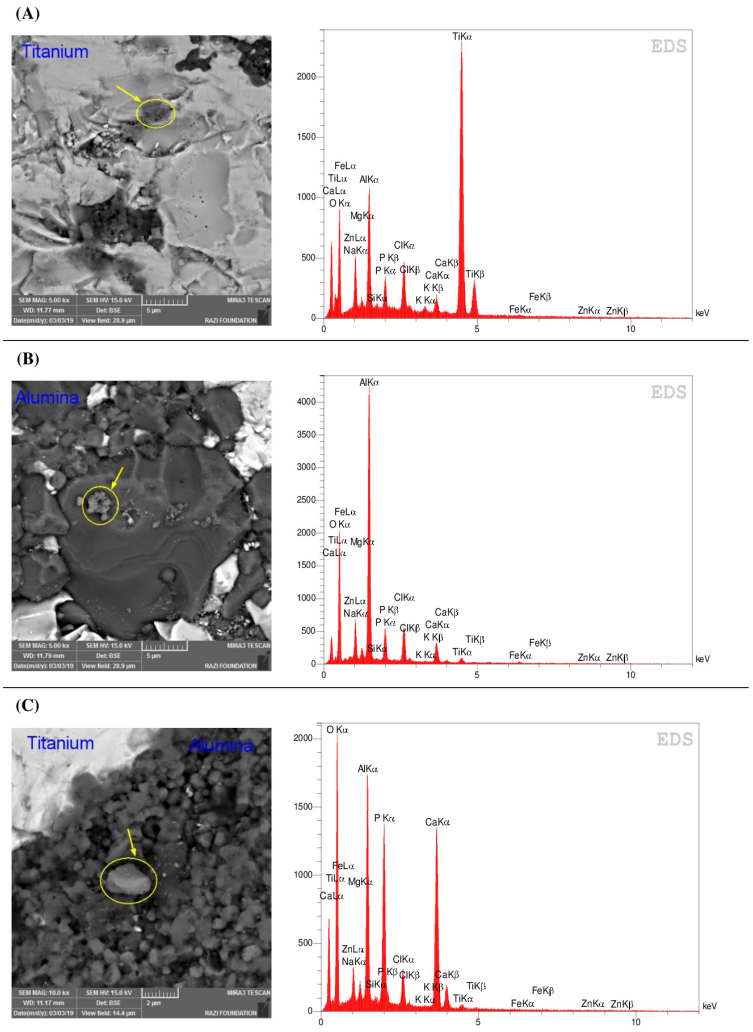

Fig. 2. SSEM and EDS analysis of (A) 75Ti, (B) 50Ti, and (C) 25Ti after 20 days of immersion in SBF.

with 50Ti (mean value of 53.66°) followed by 25Ti (mean value of 70.28°). However, 100Ti, 75Ti, and 0Ti had higher CAs (89.45°, 92.88°, and 92.07°, respectively). The Games-Howell pairwise test was run to identify the significant differences between the studied groups. The significant differences between the groups are also shown in Fig. 5a, where the means that do not share a letter are significantly different. Therefore, 50Ti and 25Ti were significantly different from each other, and from other materials (i.e., 100Ti, 75Ti, and 0Ti). However, differences between 100Ti, 75Ti, and 0Ti were not statistically significant. The results of drop width and height were also in agreement with the contact angle where the largest drop width and lowest drop height were obtained on the surfaces of 50Ti composite (Figs. 5b and 5c). Furthermore, based on the ANOVA results, the material was a significant factor on drop width ($P=0.002$) and height ($P=0.000$). Generally, if the water CA is <90°, the material surface is considered hydrophilic, meaning that a water droplet can more spread on its surface resulting in a large drop width and a low drop height. In contrast, when the water CA is >90°, the material surface is known as hydrophobic having a low drop width and a high drop height. Therefore, 50Ti and 25Ti showed hydrophilic surface properties while other fabricated materials had hydrophobic surface characteristic.

Cell viability to the materials

One-way ANOVA was employed to evaluate the viability of MC3T3-E1 cells exposed to the fabricated materials. The material was found to be a significant factor ($P=0.000$) meaning that the composition of studied materials influenced the cell viability. Fig. 6A shows the mean and STDV values of cell viability (%) with statistical differences among the groups. Considering cell viability above 80%, 75Ti, 50Ti, and 0Ti rejected any cytotoxic effect. The least viability was related to exposure to 100Ti. The viability (%) of 100Ti was below the limit line meaning that the 100Ti has cytotoxicity effect, followed by 25Ti. Furthermore, Games-Howell pairwise comparisons showed the cell viability to 75Ti (mean value of 95.01%) was significantly higher than other materials except for 0Ti (mean value of 89.90), and the cell viability to 50Ti (mean value of 87.26%) was significantly higher than

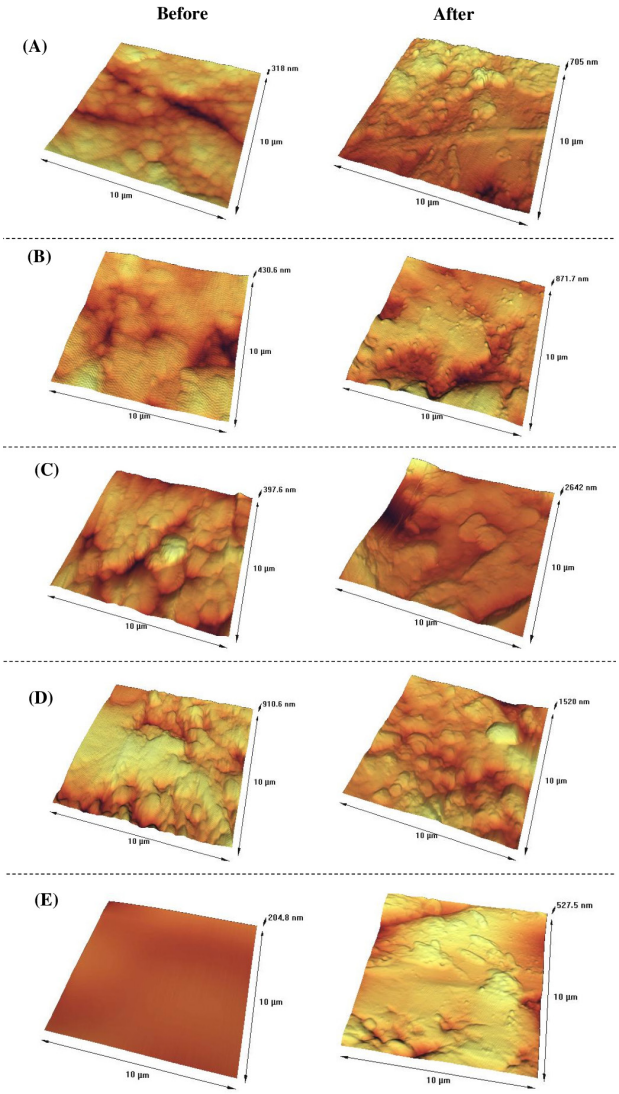

Fig. 3. AFM images of the material surfaces; (A) 100Ti, (B) 75Ti, (C) 50Ti, (D) 25Ti, and (E) 0Ti before and after 20 days of immersion in SBF.

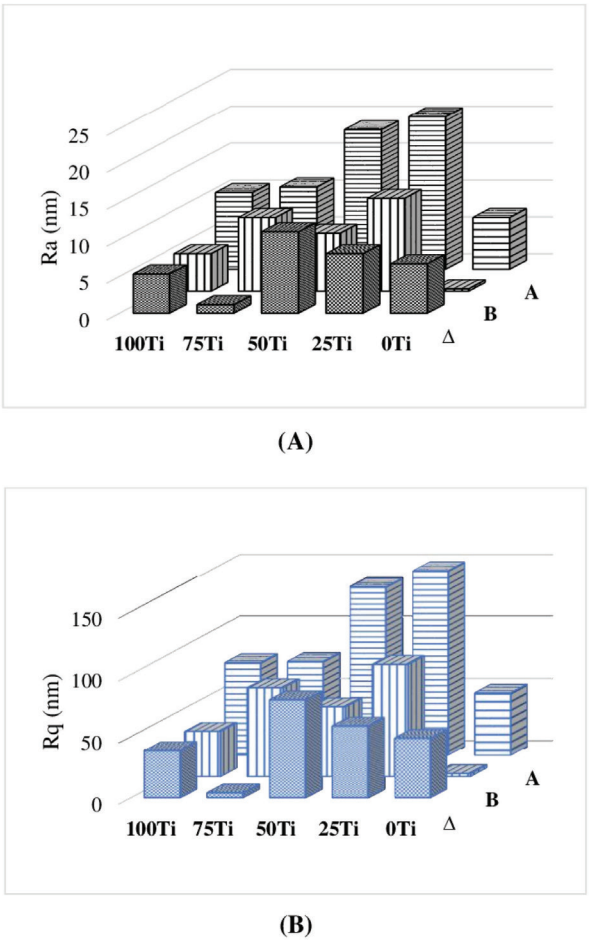

Fig. 4. The roughness values of the material surfaces; (A) Ra, and (B) Rq before and after 20 days of immersion in SBF.

25Ti (mean value of 63.89%) and 100Ti (mean value of 42.70%).

Cell proliferation

MC3T3-E1 cell proliferation cultured onto the fabricated materials was evaluated using MTT assay after 3, 7, and 10 days. Fig. 6B illustrates the means and STDVs of proliferation (%) of the studied materials. It can be seen from Fig. 6B that at early exposure (day 3) of the cells to the materials, the proliferation rate was very high (mean proliferation (%) of 215.5, 188.3, 252.3, 200.5, and 214.1 respectively for 100Ti, 75Ti, 50Ti, 25Ti, and 0Ti). The maximum proliferation was related to 50Ti. However, after 7 and 10 days of culture, the trend of proliferation was changed and the cells cultured onto 75Ti provides the highest proliferation (%) (66.9 and 89.9 after 7 and 10 days, correspondingly). Statistical analysis (two-way ANOVA) was run only for data of day 7 and day 10, as the whole data did not have normal distribution because of the very high values related to day 3. The ANOVA results indicated that both materials and time (*P* values of 0.000) were significant factors in cell proliferation (%). Tukey pairwise analysis was also carried out which indicated the proliferation (%) associated with 75Ti after 10 days was significantly higher than those of other groups after 7 and 10 days (small bar chart in Fig. 6B). Furthermore, proliferation (%) associated with this material after 7 days was significantly higher than those of other groups in the same time point. Optical micrographs were also taken after 10 days which are shown in Fig. 7. It can be seen from this figure that the cells in contact with 75Ti were numerous and provided very dense layer. The cells exposed to 50Ti formed a uniform monolayer, but the layer was not as dense as that of 75Ti. In 25Ti, however, the cell layer was uneven so that cell accumulation sites and large free spaces were observed. Furthermore, cells cultured onto 100Ti and 0Ti provided a layer of lower density with free spaces.

Cell differentiation and matrix mineralization

ALP assay was used to evaluate the differentiation from

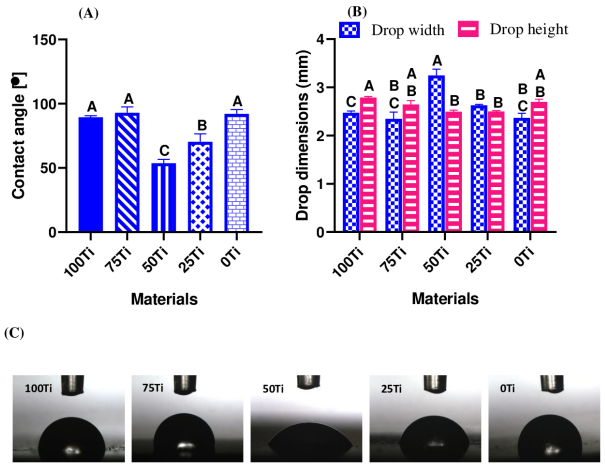

Fig. 5. Wettability results; (A) contact angle, (B) drop width and height, and (C) drop shape

pre-osteoblasts to osteoblasts (the osteogenic function) of MC3T3-E1 cells exposed to the fabricated materials at three-time intervals. ALP activity of different groups was similar, while the ALP activity increased by the culture time (Fig. 6C). As it can be seen in Fig. 6C, at day 7, the ALP concentration rapidly increased up to day 14. Nevertheless, the increase of ALP concentration occurred in a lower degree from day 14 to day 21. Two-way ANOVA also revealed that material was not a significant factor ($P = 0.083$) on ALP activity, but time (P value=0.000) was. The statistical analysis also showed significant differences between different time points, but not between the tested materials.

To determine the mineralization and calcium deposit, MC3T3-E1 cells were seeded and maintained in the osteogenic cell culture medium for 7 and 14 days, and the samples were stained using calcium staining Alizarin Red kit. Fig. 8A shows the Alizarin Red staining of different materials after osteogenic induction for 7 and 14 days, and Fig. 8B shows the percentages of red-stained area on the discs. As it can be observed, the red-stained area was found on the surfaces of all samples. The highest mineralization was seen on the surface of 25Ti, followed by 50Ti. The mineralized area was increased by time on 100Ti, 75Ti, 50Ti, and 0Ti.

Adhesion of cells to the material surface

The capability of the studied materials on cell adhesion was inferred by SEM images. Fig. 9 clearly shows that the morphology of adhered cells on different substrates was dissimilar. The cells were quite spindle-shape on 100Ti, and slightly enlarged on 75Ti where more pseudopodia and dendritic shape were observed. This means that 75Ti had better ability for cell adhesion rather than 100Ti. Furthermore, the cells stretched and enlarged multi-directionally on the surfaces of 50Ti, 25Ti, and 0Ti, particularly on 50Ti with long pseudopodia (Fig. 9C right image). The cytoplasmic extensions and interconnected

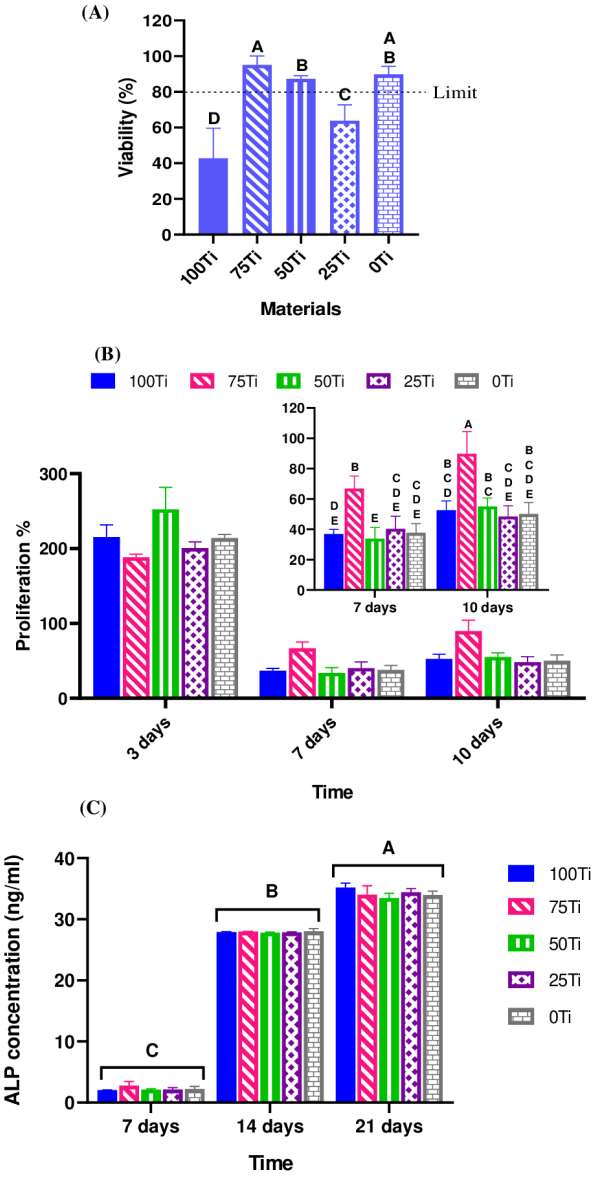

Fig. 6. Mean ± SD values of (A) cell viability, (B) proliferation (%), and (C) ALP concentrations.

adhered cells present good adhesion morphology,[27,28] thus 50Ti exhibited better cell adhesion. The pseudopodia and interconnectivity, however, were lower for 25Ti and 0Ti, respectively.

Discussion

The apatite formation ability of a material surface in an SBF solution may preliminary indicate the in-vivo bone bioactivity of that material.[23] The materials developed here with potential applications in replacements of high load-bearing joints such as hip and knee, need to possess bone-bonding ability at their interfaces with the bony bed, particularly if they would be fixed without bone cement. Our results indicated that all materials performed similarly and mostly with Ca/P below the identified range of natural bone. Therefore, to improve their

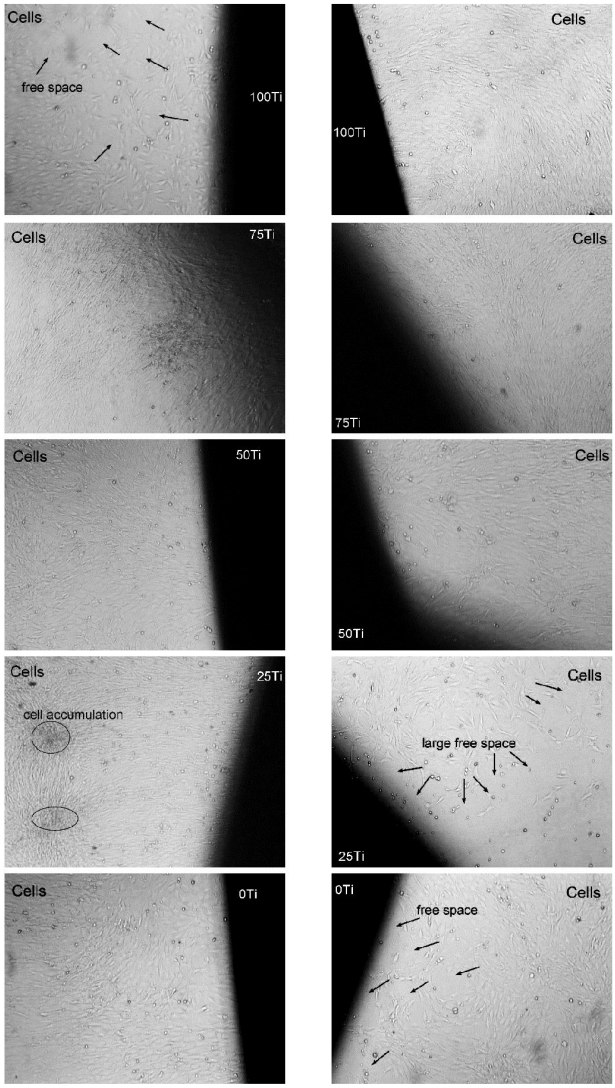

Fig. 7. Optical images of the cells cultured onto the materials at day 10 (×40)

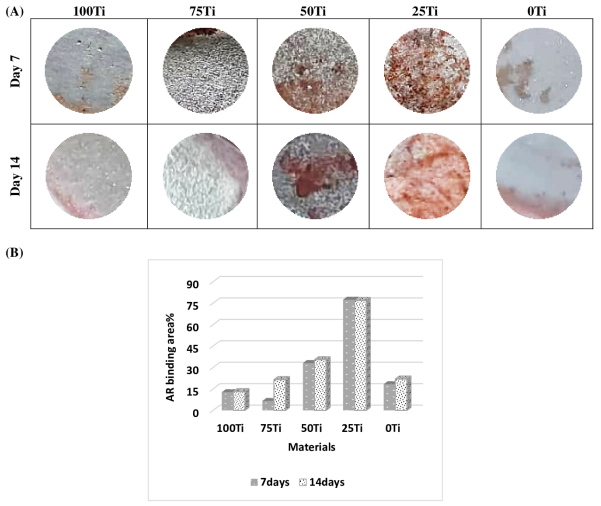

Fig. 8. (A) Alizarin Red-stained samples after 7 and 14 days, and (B) percentages of the red-stained area.

apatite formation ability, surface treatment is a possible way forward. Previous studies showed that pure Ti and alumina-based materials have low apatite formation ability, however applying surface treatments can enhance the bioactivity.[29-32] For example, Kim et al[29] conducted NaOH treatment of pure Ti alone, and along with heat treatment at 600°C, which resulted in the formation of sodium titanate having a smooth graded structure on Ti. This layer provided a smooth graded apatite layer on the Ti metal substrates in SBF. Another approach for treatment of Ti was anodic oxidation in H_2SO_4 solution[30] which caused the formation of anatase and rutile on Ti surface inducing apatite formation when soaked in SBF. On the other hand, alumina-based materials could be treated using aqueous solution of $Mg(H_2PO_4)_2$, $Ca(NO_3)_2$, and $CaCl_2$ to induce apatite formation. The treated 3Y-TZP was found to be more bioactive than 12Ce-TZP, and alumina, respectively.[31] The bioactivity of porous alumina was also enhanced by decorating bioactive $CaO–SiO_2–Ag_2O$ glass materials onto and into nano-pores by a simple sol-dipping technique.[32] Therefore, for the fabricated composites here, a hybrid surface treatment seems to be required to modify Ti and alumina concurrently and provide Ca/P ratio in the order of human natural bone.

The results of AFM and surface roughness showed rougher and non-uniform surfaces after immersion in SBF which can be attributed to the deposition of minerals on the surfaces and the corrosion phenomenon occurred in the solution for metallic phase.[20] This is in agreement with the wettability values obtained, where 50Ti and 75Ti respectively with the lowest and highest CAs (the highest and lowest wettability), had the largest and smallest ΔRa and ΔRq. The high wettability means the material has hydrophilic high-energy surface resulting in strong molecular attraction. Therefore, higher mineral adsorption on 50Ti surface can be attributed to its hydrophilicity which may attract more minerals and provide rougher and more non-uniform surface meaning that larger ΔRa and ΔRq. Guzman et al[22] who measured the CAs of pure alumina and a composite with 25vol.% Ti found that the CA of the composite surface was lower than that of alumina, which supports our finding.

The cytotoxic potential of the materials was assessed by analyzing the activity of LDH enzyme released from the damaged cells. The higher the LDH concentration released into the medium, the higher the cellular membrane damage. This means higher cytotoxicity of the materials and lower viability of the cells. Materials with cytotoxicity below 20% (viability above 80%) are usually considered to have almost no changes in the cell membrane.[22, 33] Therefore, 75Ti, 50Ti, and 0Ti are considered non-toxic. Furthermore, the results of MTT assay on 50Ti showed high cell proliferation at early stage while the cells exposed to 75Ti proliferated more at later stages. Surprisingly, the percentages obtained by MTT at day 3 showed high cell proliferation which do

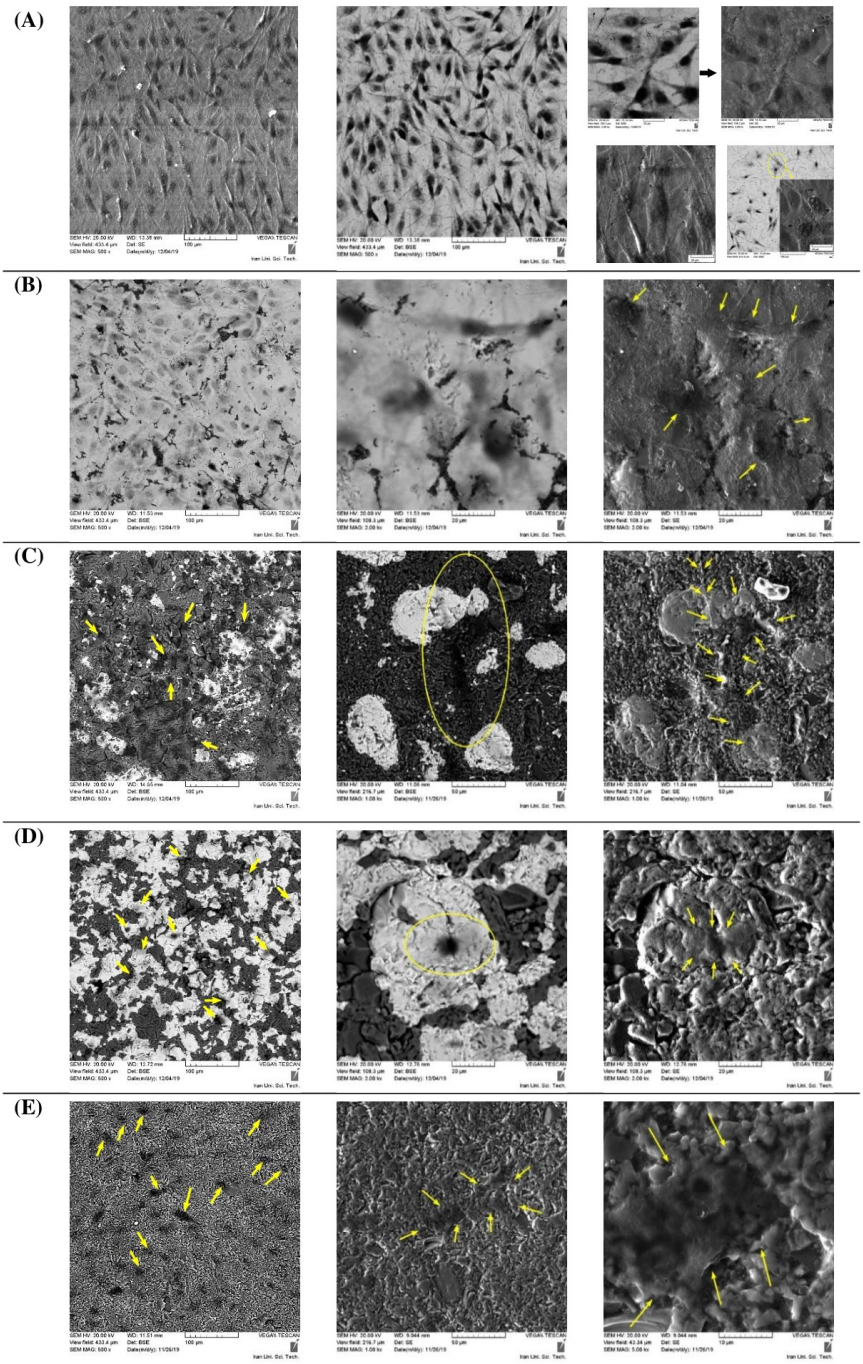

Figure 9. SEM images of the adhered cells on different materials; (A) 100Ti, (B) 75Ti, (C) 50Ti, (D) 25Ti, and (E) 0Ti

not correspond with the observations resulting from the LDH after 3 days of exposure. One possible explanation is that the testing materials act as metabolic enhancers. Therefore, despite the lower number of viable cells (as determined by the LDH test), the conversion of MTT into formazan was enhanced, leading to the overestimated cell proliferation.[34] The difference observed in the results of MTT and LDH assays emphasizes the need to carry out various tests to make an appropriate conclusion on the safety of biomaterials. The cell proliferation percentage above 100% resulted from MTT assay (similar to the present study) has been observed in other studies for different biomaterials including Ti.[35,36] The proliferation percentages became lower by time suggesting that the effect of studied materials on cell metabolism was higher at the early exposure. The viability obtained here for alumina (0Ti) is in agreement with[22] in which viability of 80%< for alumina was reported under the same testing condition. However, their results on 25vol.% Ti composite was different from ours. Furthermore, in many studies the cytotoxicity of Ti was assessed usually as a benchmark material to be compared with the newly developed or

surface-modified biomaterials.[37-41] For example, Hahn et al[37] conducted LDH cytotoxicity assay on MC3T3-E1 after 24-hour culture on Ti, HA coating, and HA-CNT coating for which the cytotoxicity of 57.6% was obtained for Ti.

Differentiated osteoblasts are capable of producing ALP and depositing calcium (extracellular matrix mineralization). Osteoblasts are specific fibroblasts which are derived from mesenchymal precursors. These cells secrete, precipitate, and mineralize the bone matrix. In fact, their differentiation includes cell proliferation, matrix maturation, and matrix mineralization, respectively.[42] When the mineralization is completed, calcium deposition can be detected by Alizarin Red staining. Calcium forms an Alizarin Red S-calcium complex which provides a bright red stain. The studied composites showed higher matrix mineralization compared with 0Ti and 100Ti (the pure form of Ti and Al_2O_3). However, cell differentiation based on ALP activity showed that all fabricated materials had similar performance (no statistical difference). This indicates the necessity of conducting these two tests together to better understand the material osteogenic performance. Another issue is that the osteogenic factors used here, for the differentiation of MC3T3-E1 were ascorbic acid and β-glycerophosphate, which have been commonly implemented to make osteogenic medium for these cells.[43-46] Nevertheless, some studies have additionally used dexamethasone,[33,47] that has been avoided to be used due to its toxic effect on the cells, in many studies. However, it would be beneficial to investigate the effect of this osteogenic factor on differentiation of MC3T3-E1 cells, particularly in evaluation of ALP activity.

Different cellular interactions were identified on the surfaces of the tested materials. This might be due to the variations in chemical composition, surface topography, and wettability[48,49] because the adhesion of cells initiates with the physical/chemical attachment of the cells on the material surface[50] and the early interaction zone with cells narrows to an atomic layer on the surface. Three processes occur successively after a biomaterial implantation.[51] First, ions and water molecules reach the surface which interact and bind differently depending upon the biomaterial surface properties such as hydrophobicity. This influences the attachment of proteins and other molecules, which arrive a little later. For example, water-soluble proteins which have hydration shells interact with the surface water layer. This would affect the structures of the protein adlayers such as denaturation, orientation, and coverage. These structures are realized by the cells arrived at the surface to adhere, spread, and form an interface on the biomaterial surface. Consequently, the surface properties and structures of the protein adlayers highly influence the initial cell adhesion. The superior cell adhesion capability of 50Ti, therefore, can be explained by its low contact angle, that is high wettability or hydrophilicity. 25Ti also had low contact angle (higher than 50Ti), thus its surface could show good cell adhesion but in a lower degree than 50Ti, as observed in SEM images. Other studies also investigated the adhesion of MC3T3-E1 cells on pure Ti substrate and found spindle-shaped configuration,[52-54] similar to the present study. Fernandez-Garcia et al[33] assessed the biological interaction of a set of ZrO_2-Ti composites and measured the surface area of the adhered cells on different materials. They found the lowest cell surface area on pure Ti meaning that the cells could not stretch and enlarge on Ti surface. This is in agreement with our result on pure Ti. To further analyse the morphology of cells and the cytoskeleton organization of MC3T3-E1 on the samples, fluorescent staining of the adhered cells can be done. It would be interesting for future research to stain the F-actin and nuclei of the cells for example by FITC-phalloidin and DAPI, and analyse them by confocal laser scanning microscope. This helps in better realizing the cytoskeleton structure of the adhered cells and provides insights on the cell differentiation.[43,55]

Research Highlights

What is the current knowledge?

√ Ti implants suffer from several shortcomings, thus composite materials are being developed.

√ Al_2O_3-Ti composites have been shown to have superior mechanical and corrosion behaviour.

√ Al_2O_3-Ti composites require to be examined for their biocompatibility to ensure safe use.

√ In-vitro cytotoxicity of spark plasma sintered Al_2O_3, Ti and Al_2O_3-Ti composites was assessed.

What is new here?

√ Cell viability and proliferation was highest in exposure to 75Ti and 50Ti composites.

√ Cell adhesion was better on the composites and Al_2O_3, particularly 50Ti, rather than Ti.

Conclusion

All materials were processed under the same procedure, however, they presented different surface characteristics due to the difference in composition. Apatite formation test showed that both Ca and P deposited on the surfaces of all materials. However, Ca/P ratio in most of the regions obtained after 20 days of immersion in SBF were below the identified value in natural bones. Cell viability to 75Ti, 50Ti, and 25Ti was superior when compared with 100Ti. Furthermore, 50Ti showed high cell proliferation at early stage while the cells exposed to 75Ti proliferated more at later stages. The cells adhered differently on different materials where more spindle-shaped configuration was found on 100Ti and more enlarged cells on 0Ti, 25Ti, 50Ti, and 75Ti. The matrix mineralization was also different on the surfaces of different materials. 25Ti showed high mineralized area, followed by 50Ti.

In summary our findings demonstrated that 75Ti, 50Ti, and 25Ti have high potential to be used as load-bearing

orthopedic materials. However, more analyses based on the animal tests are required.

Acknowledgments
The authors would like to thank Semnan University of Medical Sciences for funding this work (No. 1310).

Funding sources
This study was funded by Semnan University of Medical Sciences (NO. 1310).

Ethical statement
This article does not contain any studies with human participants or animals performed by any of the authors.

Competing interests
The authors declare that they have no conflict of interests.

Authors' contribution
MB: conceptualization, data analysis, provision of study materials and equipment, draft preparation, writing and reviewing. SA: experiment design, writing and reviewing. SG: experiment design.

References

1. Winkler T, Sass F, Duda G, Schmidt-Bleek K. A review of biomaterials in bone defect healing, remaining shortcomings and future opportunities for bone tissue engineering: The unsolved challenge. *Bone Joint J* **2018**; 7: 232-43. https://doi.org/10.1302/2046-3758.73.BJR-2017-0270.R1
2. Kalpana S K. Biomaterials in total joint replacement. *Colloids Surf B Biointerfaces* **2004**; 39: 133-42. https://doi.org/10.1016/j.colsurfb.2003.12.002
3. Köse N. Biological response to orthopedic implants and biomaterials. In: Korkusuz F, eds. *Musculoskeletal Research and Basic Science*. Cham: Springer; **2016**. p. 3-14. https://doi.org/10.1007/978-3-319-20777-3_1
4. Vallet-Regí M, Salinas AJ. 6 - Ceramics as bone repair materials. In: Pawelec KM, JA Planell, eds. *Bone Repair Biomaterials (Second Edition)*: Woodhead Publishing; **2019**. p. 141-78. https://doi.org/10.1016/B978-0-08-102451-5.00006-8
5. Bahraminasab M, Edwards KL. Biocomposites for Hard Tissue Replacement and Repair. In: Sidhu S. BP, Zitoune R, Yazdani M, eds. *Futuristic Composites Materials Horizons: From Nature to Nanomaterials,*. Singapore: Springer; **2018**. p. 281-96.
6. Affatato S, Jaber SA, Taddei P. Ceramics for Hip Joint Replacement. In: Zivic F, S Affatato, M Trajanovic, M Schnabelrauch, N Grujovic, KL Choy, eds. *Biomaterials in Clinical Practice : Advances in Clinical Research and Medical Devices*. Cham: Springer International Publishing; **2018**. p. 167-81. https://doi.org/10.1007/978-3-319-68025-5_7
7. Bahraminasab M, Sahari BB, Edwards KL, Farahmand F, Arumugam M, Hong TS. Aseptic loosening of femoral components - a review of current and future trends in materials used. *Mater Des* **2012**; 42: 459–70. https://doi.org/10.1016/j.matdes.2012.05.046
8. Bahraminasab M, Farahmand F. State of the art review on design and manufacture of hybrid biomedical materials: Hip and knee prostheses. *Proc Inst Mech Eng [H] J Eng Med* **2017**; 231: 1-29. https://doi.org/10.1177/0954411917705911
9. Swiatkowska I, Martin N, Hart AJ. Blood titanium level as a biomarker of orthopaedic implant wear. *J Trace Elem Med Biol* **2019**; 53: 120-8. https://doi.org/10.1016/j.jtemb.2019.02.013
10. Alves SA, Beline T, Barão VAR, Sukotjo C, Mathew MT, Rocha LA, et al. Chapter 3 - Degradation of titanium-based implants. In: Souza JCM, D Hotza, B Henriques, AR Boccaccini, editors. *Nanostructured Biomaterials for Cranio-Maxillofacial and Oral Applications*: Elsevier; **2018**. p. 41-62. https://doi.org/10.1016/B978-0-12-814621-7.00003-2
11. Mombelli A, Hashim D, Cionca N. What is the impact of titanium particles and biocorrosion on implant survival and complications? A critical review. *Clin Oral Implants Res* **2018**; 29: 37-53. https://doi.org/10.1111/clr.13305
12. Chevalier J, Gremillard L. Ceramics for medical applications: a picture for the next 20 years. *J Eur Ceram Soc* **2009**; 29: 1245-55. https://doi.org/10.1016/j.jeurceramsoc.2008.08.025
13. Bergschmidt P, Bader R, Kluess D, Zietz C, Mittelmeier W. The All-Ceramic Knee Endoprosthesis-The Gap Between Expectation and Experience with Ceramic Implants. *Semin Arthroplasty* **2012**; 23: 262-7. https://doi.org/10.1053/j.sart.2013.01.010
14. Bahraminasab M, Sahari BB, Edwards KL, Farahmand F, Arumugam M. Aseptic loosening of femoral components-materials engineering and design considerations. *Mater Des* **2013**; 44: 155-63. https://doi.org/10.1016/j.matdes.2012.07.066
15. Bahraminasab M, Ghaffari S, Eslami-Shahed H. Al2O3-Ti functionally graded material prepared by spark plasma sintering for orthopaedic applications. *J Mech Behav Biomed Mater* **2017**; 72: 82-9. https://doi.org/10.1016/j.jmbbm.2017.04.024
16. Gutierrez-Gonzalez CF, Fernandez-Garcia E, Fernandez A, Torrecillas R, Lopez-Esteban S. Processing, spark plasma sintering, and mechanical behavior of alumina/titanium composites. *J Mater Sci* **2014**; 49: 3823-30. https://doi.org/10.1007/s10853-014-8095-5
17. Hayun S, Meir S, Kalabukhov S, Frage N, Zaretsky E. Phase Constitution and Dynamic Properties of Spark Plasma-Sintered Alumina–Titanium Composites. *J Am Ceram Soc* **2015**; 99: 573-80. https://doi.org/10.1111/jace.13992
18. Meir S, Kalabukhov S, Frage N, Hayun S. Mechanical properties of Al 2 O 3\ Ti composites fabricated by spark plasma sintering. *Ceram Int* **2015** 41: 4637-43. https://doi.org/10.1016/j.ceramint.2014.12.008
19. Fujii T, Tohgo K, Iwao M, Shimamura Y. Fabrication of alumina-titanium composites by spark plasma sintering and their mechanical properties. *J Alloys Compd* **2018** 744: 759-68. https://doi.org/10.1016/j.jallcom.2018.02.142
20. Bahraminasab M, Bozorg M, Ghaffari S, Kavakebian F. Corrosion of Al2O3-Ti composites under inflammatory condition in simulated physiological solution. *Mater Sci Eng C Mater Biol Appl* **2019** 102: 200-11. https://doi.org/10.1016/j.msec.2019.04.047
21. Bahraminasab M, Bozorg M, Ghaffari S, Kavakebian F. Electrochemical corrosion of Ti-Al2O3 biocomposites in Ringer's solution. *J Alloys Compd* **2019** 777: 34-43. https://doi.org/10.1016/j.jallcom.2018.09.313
22. Guzman R, Fernandez-García E, Gutierrez-Gonzalez CF, Fernandez A, Lopez-Lacomba JL, Lopez-Esteban S. Biocompatibility assessment of spark plasma-sintered alumina-titanium cermets. *J Biomater Appl* **2016**; 30: 759-69. https://doi.org/10.1177/0885328215584858
23. Kokubo T, Takadama H. How useful is SBF in predicting in vivo bone bioactivity? *Biomaterials* **2006**; 27: 2907-15. https://doi.org/10.1016/j.biomaterials.2006.01.017
24. Menzies KL, Jones L. The impact of contact angle on the biocompatibility of biomaterials. *Optom Vis Sci* **2010**; 87: 387-99. http://dx.doi.org/10.1097/OPX.0b013e3181da863e
25. Bahraminasab M, Arab S, Jahan A. Adaptation of MC3T3 cell line to Dulbecco's Modified Eagle's medium. *Tissue Cell* **2020** 64: 101341. https://doi.org/10.1016/j.tice.2020.101341
26. Sotiropoulou P, Fountos G, Martini N, Koukou V, Michail C, Kandarakis I, et al. Bone calcium/phosphorus ratio determination using dual energy X-ray method. *Physica Medica* **2015**; 31: 307-13. https://doi.org/10.1016/j.ejmp.2015.01.019
27. Shuai C, Zan J, Yang Y, Peng S, Yang W, Qi F, et al. Surface modification enhances interfacial bonding in PLLA/MgO bone scaffold. *Mater Sci Eng C Mater Biol Appl* **2020**; 108: 110486. https://doi.org/10.1016/j.msec.2019.110486
28. Shuai C, Yang W, Yang Y, Pan H, He C, Qi F, et al. Selective laser melted Fe-Mn bone scaffold: microstructure, corrosion behavior and cell response. *Mater Res Express* **2020**; 7: 015404. https://doi.org/10.1088/2053-1591/ab62f5
29. Kim HM, Miyaji F, Kokubo T, Nishiguchi S, Nakamura T.

Graded surface structure of bioactive titanium prepared by chemical treatment. *J Biomed Mater Res* **1999**; 45: 100-7. https://doi.org/10.1002/(SICI)1097-4636(199905)45:2<100::AID-JBM4>3.0.CO;2-0

30. Yang B, Uchida M, Kim H-M, Zhang X, Kokubo T. Preparation of bioactive titanium metal via anodic oxidation treatment. *Biomaterials* **2004**; 25: 1003-10. https://doi.org/10.1016/S0142-9612(03)00626-4
31. Dehestani M, Zemlyanov D, Adolfsson E, Stanciu LA. Improving bioactivity of inert bioceramics by a novel Mg-incorporated solution treatment. *Appl Surf Sci* **2017**; 425: 564-75. https://doi.org/10.1016/j.apsusc.2017.07.009
32. Ni S, Li X, Yang P, Ni S, Hong F, Webster TJ. Enhanced apatite-forming ability and antibacterial activity of porous anodic alumina embedded with CaO–SiO2–Ag2O bioactive materials. *Mater Sci Eng C Mater Biol Appl* **2016**; 58: 700-8. https://doi.org/10.1016/j.msec.2015.09.011
33. Fernandez-Garcia E, Guillem-Marti J, Gutierrez-Gonzalez CF, Fernandez A, Ginebra MP, Lopez-Esteban S. Osteoblastic cell response to spark plasma-sintered zirconia/titanium cermets. *J Biomater Appl* **2014**; 29: 813-23. https://doi.org/10.1177/0885328214547400
34. Braz L, Grenha A, Ferreira D, Rosa da Costa AM, Gamazo C, Sarmento B. Chitosan/sulfated locust bean gum nanoparticles: In vitro and in vivo evaluation towards an application in oral immunization. *Int J Biol Macromol* **2017**; 96: 786-97. https://doi.org/10.1016/j.ijbiomac.2016.12.076
35. Park JW, Suh JY, Chung HJ. Effects of calcium ion incorporation on osteoblast gene expression in MC3T3-E1 cells cultured on microstructured titanium surfaces. *J Biomed Mater Res Part A* **2008**; 86: 117-26. https://doi.org/10.1002/jbm.a.31618
36. Myung SW, Ko YM, Kim BH. Effect of plasma surface functionalization on preosteoblast cells spreading and adhesion on a biomimetic hydroxyapatite layer formed on a titanium surface. *Appl Surf Sci* **2013**; 287: 62-8. https://doi.org/10.1016/j.apsusc.2013.09.064
37. Hahn B-D, Lee J-M, Park D-S, Choi J-J, Ryu J, Yoon W-H, et al. Mechanical and in vitro biological performances of hydroxyapatite–carbon nanotube composite coatings deposited on Ti by aerosol deposition. *Acta Biomater* **2009**; 5: 3205-14. https://doi.org/10.1016/j.actbio.2009.05.005
38. Li M, Ren L, Li L, He P, Lan G, Zhang Y, et al. Cytotoxic Effect on Osteosarcoma MG-63 Cells by Degradation of Magnesium. *J Mater Sci Technol* **2014**; 30: 888-93. https://doi.org/10.1016/j.jmst.2014.04.010
39. McMahon RE, Ma J, Verkhoturov SV, Munoz-Pinto D, Karaman I, Rubitschek F, et al. A comparative study of the cytotoxicity and corrosion resistance of nickel–titanium and titanium–niobium shape memory alloys. *Acta Biomater* **2012**; 8: 2863-70. https://doi.org/10.1016/j.actbio.2012.03.034
40. Benko A, Wiecheć A, Rajchel B, Długoń E, Błażewicz M. Titanium Surface Modification with Carbon Nanotubes. Towards Improved Biocompatibility. *Acta Phys Pol* **2016**; 129: 176-8. https://doi.org/10.12693/APhysPolA.129.176
41. Wang T, Qian S, Zha G-C, Zhao X-J, Ding L, Sun J-Y, et al. Synergistic effects of titania nanotubes and silicon to enhance the osteogenic activity. *Colloids Surf B Biointerfaces* **2018**; 171: 419-26. https://doi.org/10.1016/j.colsurfb.2018.07.052
42. de Lima Cavalcanti JH, Matos PC, Depes de Gouvêa CV, Carvalho W, Calvo-Guirado JL, Aragoneses JM, et al. In Vitro Assessment of the Functional Dynamics of Titanium with Surface Coating of Hydroxyapatite Nanoparticles. *Materials* **2019**; 12: 840. https://doi.org/10.3390/ma12050840
43. Degli Esposti M, Chiellini F, Bondioli F, Morselli D, Fabbri P. Highly porous PHB-based bioactive scaffolds for bone tissue engineering by in situ synthesis of hydroxyapatite. *Mater Sci Eng C Mater Biol Appl* **2019**; 100: 286-96. https://doi.org/10.1016/j.msec.2019.03.014
44. St-Pierre J-P, Gauthier M, Lefebvre L-P, Tabrizian M. Three-dimensional growth of differentiating MC3T3-E1 pre-osteoblasts on porous titanium scaffolds. *Biomaterials* **2005**; 26: 7319-28. https://doi.org/10.1016/j.biomaterials.2005.05.046
45. Jarrahy R, Huang W, Rudkin GH, Lee JM, Ishida K, Berry MD, et al. Osteogenic differentiation is inhibited and angiogenic expression is enhanced in MC3T3-E1 cells cultured on three-dimensional scaffolds. *Am J Physiol Cell Physiol* **2005**; 289: C408-C14. https://doi.org/10.1152/ajpcell.00196.2004
46. Li Y, Kim JH, Choi EH, Han I. Promotion of osteogenic differentiation by non-thermal biocompatible plasma treated chitosan scaffold. *Sci Rep* **2019**; 9: 1-10. https://doi.org/10.1038/s41598-019-40371-6
47. Sayed S, Faruq O, Hossain M, Im S-B, Kim Y-S, Lee B-T. Thermal cycling effect on osteogenic differentiation of MC3T3-E1 cells loaded on 3D-porous Biphasic Calcium Phosphate (BCP) scaffolds for early osteogenesis. *Mater Sci Eng C Mater Biol Appl* **2019**; 105: 110027. https://doi.org/10.1016/j.msec.2019.110027
48. Chen S, Guo Y, Liu R, Wu S, Fang J, Huang B, et al. Tuning surface properties of bone biomaterials to manipulate osteoblastic cell adhesion and the signaling pathways for the enhancement of early osseointegration. *Colloids Surf B Biointerfaces* **2018**; 164: 58-69. https://doi.org/10.1016/j.colsurfb.2018.01.022
49. Spriano S, Chandra VS, Cochis A, Uberti F, Rimondini L, Bertone E, et al. How do wettability, zeta potential and hydroxylation degree affect the biological response of biomaterials? *Mater Sci Eng C Mater Biol Appl* **2017**; 74: 542-55. https://doi.org/10.1016/j.msec.2016.12.107
50. Sackmann E, Smith A-S. Physics of cell adhesion: some lessons from cell-mimetic systems. *Soft Matter* **2014**; 10: 1644-59. https://doi.org/10.1039/C3SM51910D
51. Tagaya M, Ikoma T, Hanagata N, Tanaka J. Analytical investigation of protein mediation between biomaterials and cells. *Mater Express* **2012**; 2: 1-22. https://doi.org/10.1166/mex.2012.1053
52. Zhang Z, Gu B, Zhang W, Kan G, Sun J. The enhanced characteristics of osteoblast adhesion to porous Zinc–TiO2 coating prepared by plasma electrolytic oxidation. *Appl Surf Sci* **2012**; 258: 6504-11. https://doi.org/10.1016/j.apsusc.2012.03.067
53. Ma A, Shang H, Song Y, Chen B, You Y, Han W, et al. Icariin-functionalized coating on TiO2 nanotubes surface to improve osteoblast activity in vitro and osteogenesis ability in vivo. *Coatings* **2019**; 9: 1-17. https://doi.org/10.3390/coatings9050327
54. Zhang W, Gu J, Zhang C, Xie Y, Zheng X. Preparation of titania coating by induction suspension plasma spraying for biomedical application. *Surf Coat Technol* **2019**; 358: 511-20. https://doi.org/10.1016/j.surfcoat.2018.11.047
55. Whitelock JM, Melrose J. Adhesion of Cells to Biomaterials. *Wiley Encyclopedia of Biomedical Engineering* **2006**. https://doi.org/10.1002/9780471740360.ebs0028